Bull Volcanol (2001) 63:61–72
DOI 10.1007/s004450000122

RESEARCH ARTICLE

Franck Donnadieu · Olivier Merle
Jean-Claude Besson

Volcanic edifice stability during cryptodome intrusion

Received: 6 January 2000 / Accepted: 8 December 2000 / Published online: 1 February 2001

Abstract Limit equilibrium analyses were applied to the 1980 Mount St. Helens and 1956 Bezymianny failures in order to examine the influence on stability of structural deformation produced by cryptodome emplacement. Weakening structures associated with the cryptodome include outward-dipping normal faults bounding a summit graben and a flat shear zone at the base of the bulged flank generated by lateral push of the magma. Together with the head of the magmatic body itself, these structures serve directly to localize failure along a critical surface with low stability deep within the interior of the edifice. This critical surface, with the safety coefficient reduced by 25–30%, is then very sensitive to stability condition variation, in particular to the pore-pressure ratio (r_u) and seismicity coefficient (n). For r_u=0.3, or n=0.2, the deep surface suffers catastrophic failure, removing a large volume of the edifice flank. In the case of Mount St. Helens, failure occurred within a material with angle of friction ~40°, cohesion in the range 10^5–10^6 Pa, and probably significant water pore pressure. On 18 May 1980, detachment of slide block I occurred along a newly formed rupture surface passing through the crest of the bulge. Although sliding of block I may have been helped by the basal shear zone, significant pore pressure and a triggering earthquake were required (r_u=0.3 and n=0.2). Detachment of the second block was guided by the summit normal fault, the front of the cryptodome, and the basal shear zone. This occurred along a deep critical surface, which was on the verge of failure even before the 18 May 1980 earthquake. The stability of equivalent surfaces at Bezymianny Volcano appears significantly higher. Thus, although magma had already reached the surface, weaker materials, or higher pore pressure and/or seismic conditions were probably required to reach the rupture threshold. From our analysis, we find that deep-seated sector collapses formed by removing the edifice summit cannot generally result from a single slide. Cryptodome-induced deformation does, however, provide a deep potential slip surface. As previously thought, it may assist deep-seated sector collapse because it favors multiple retrogressive slides. This leads to explosive depressurization of the magmatic and hydrothermal systems, which undermines the edifice summit and produces secondary collapses and explosive blasts.

Keywords Avalanche · Caldera · Cryptodome · Limit equilibrium · Mount St. Helens

Editorial responsibility: M.R. Carroll

F. Donnadieu (✉) · O. Merle · J.-C. Besson
UMR 6524, Magmas and Volcans – CNRS,
Clermont-Ferrand, France
e-mail: fdonnadi@geosc.psu.edu
Tel.: +1-814-8659993, Fax: +1-814-8637823

Present address: F. Donnadieu
Department of Geosciences, 334 Deike Building,
Penn State University, University Park, PA 16803, USA

Introduction

Flank failures are part of the normal growth process of mature stratovolcanoes. There are a range of types of slope failure on composite volcanoes, ranging from those without coeval eruptions to those accompanied by explosive eruption (Siebert et al. 1987; Voight and Elsworth 1997). The former are commonly shallow, such as the seismically triggered failure at Ontake, Japan (Voight and Sousa 1994). Others, sometimes deep-seated, can be generated by gradual spreading of the substratum, which may then be incorporated in large quantities in debris avalanche deposits (van Wyk de Vries and Francis 1997). Hydrothermal alteration is one important parameter that can weaken the edifice core and sometimes cause flank spreading (van Wyk de Vries et al. 2000). It can lead to lateral collapse of the edifice, especially if combined with a physical trigger such as an earthquake. The eruption-associated failures include Bezymianny-type eruptions when a magmatic component is involved, and Banda-type eruptions when solely phreatic (Siebert et al. 1987; Voight and Elsworth 1997).

One way destabilization can occur is by cryptodome growth within the edifice, as illustrated by the 18 May 1980 collapse at Mount St. Helens (Voight et al. 1981). The event at Bezymianny Volcano on 30 March 1956 (Gorshkov 1959) has been recognized as of the same edifice-failure type (Siebert et al. 1987; Belousov and Bogoyavlenskaya 1988). Deposits possibly resulting from a similar scenario have since been recognized around many other volcanic edifices (e.g., Boudon et al. 1984; Siebert et al. 1987, 1995; Siebert 1996).

In this paper, we first review the role of, and the interactions among, the general material parameters controlling failure and not linked necessarily to the intrusion of a cryptodome. Next, the structures produced by cryptodome intrusion, as revealed by analog models (Donnadieu and Merle 1998), are taken into account. We show that these structures reduce edifice stability and promote catastrophic flank failure. Their relevance to the formation of deep-seated sector collapses ("avalanche calderas") is also examined.

The collapse of Mount St. Helens

At Mount St. Helens, the 1980 slope failure was preceded by 2 months of intense deformation that was ascribed to the intrusion of a cryptodome. A bulge was created on the northern flank of the volcano, associated with an asymmetrical summit graben (Jordan and Kieffer 1981; Lipman et al. 1981; Moore and Albee 1981; Voight et al. 1981). An earthquake of magnitude 5.2 probably triggered the failure of the swelling flank, leading to a 2.3-km^3 rockslide–avalanche. Failure occurred as block I began sliding northwards along a surface passing through the crest of the bulge, immediately followed by sliding of block II along a deeper surface passing through the southern scarp of the graben. Sudden removal of the lithostatic load provoked explosive decompression of magmatic volatiles and the hydrothermal system, producing a lateral blast immediately followed by a Plinian eruption. The cataclysmic eruption left a deep slide scar truncating the old summit.

Voight et al. (1983) concluded from limit-equilibrium stability analyses that initial failures at Mount St. Helens occurred in a material with cohesion c <6×10^5 Pa, angle of friction of about 40°, and significant pore fluid pressure and transient shear stresses from a trigger earthquake. Using a three-dimensional limit-equilibrium analysis, Reid et al. (2000) have modeled these pre-collapse conditions, including deformed topography, pore pressure and seismicity, and obtained good estimates of failure location and volume. The deformation preceding the collapse of Mount St. Helens in 1980 has been modeled numerically (Paul et al. 1987) and the structural evolution has been interpreted through analog experiments (Donnadieu and Merle 1998). From physical models the surface deformation was related to a pattern of faults at depth (Fig. 11), and a general mechanism of cryptodome emplacement by viscous indentation was proposed. Based on these analog models (Fig. 1a), cryptodome intrusions cause structural weakening in several ways (Table 1). We hereafter investigate the influence on stability of the structures created at depth by the intrusion. Different potential slip surfaces have been tested (Fig. 1b): circle C may correspond to the slide surface of block I, circles A or B to block II, surface E to the post-collapse scar profile at Mount St. Helens, and D an arbitrary deep planar surface.

Computation method for limit-equilibrium analysis

Our approach is to apply the modified Bishop procedure for slip circles used in civil engineering (Bishop 1955) to different potential failure surfaces at Mount St. Helens and Bezymianny Volcanoes, for various sets of conditions. Stability is defined by a factor of safety, Fs, computed by iterations from the ratio of resisting moments to driving moments for each vertical slice (subscript i) above the considered surface of potential failure.

$$\langle \mathrm{I} \rangle \mathrm{Fs} \langle / \mathrm{I} \rangle = \frac{\sum_{i=1}^{m} \left[\frac{(c_i + (\rho_i g h_i u_i) \tan \phi_i)}{\left(1 + \frac{\tan \alpha_i \tan \phi_i}{\langle \mathrm{I} \rangle \mathrm{Fs} \langle / \mathrm{I} \rangle}\right)} \times \left(\frac{b_i}{\cos \alpha_i} \right) \right]}{\left[\sum_{i=1}^{m} (\rho_i g h_i b_i \sin \alpha_i) + \sum \frac{M_{ext}}{R} \right]}$$

where m is the number of vertical slices (m=50 for our analysis), c the cohesion, ϕ the angle of friction, ρ the bulk density of the "rock+water" medium, *g* the gravitational acceleration, h the height of the "rock+water" column, u the pore fluid pressure ($u=\rho_{fluid} g h_{fluid}$, $\rho_{fluid} \approx$ 1000 kg m^{-3}), b the slice width, α the angle of the slip surface to the horizontal, R the radius of the slip circle, and ΣM_{ext} the sum of moments resulting from external forces, like earthquake shaking.

Pore fluid pressure is introduced by the ratio r_u, with $r_u=u/(\rho g h)$; dry materials have $r_u=0$, and $r_u>0.4$ implies a piezometric level above the ground surface. Horizontal ground accelerations have been simulated through a seismic coefficient n, expressed as a fraction of the gravitational acceleration, *g*. Although average seismic forces may vary in intensity and direction as a function of time and space during a single earthquake, n is intended to approximate the net effect of seismic waves on stability (Voight et al. 1983). The inertial force is calculated from the product of the dimensionless seismic coefficient (n)

Fig. 1 **a** Structural deformation produced by the Mount St. Helens cryptodome just before the 18 May 1980 eruption, as revealed by analog models. MSF: major shear fault produced by indentation of the edifice by the viscous magma (Donnadieu and Merle 1998). **b** Trial surfaces tested with Mount St. Helens profile. *C* may correspond approximately to the slide surface of block I, *A* or *B* to block II, *D* and *E* to deep surfaces encompassing the summit area; *E* represents approximately the scar profile after collapse. *B*, *C*, *E* redrawn from Voight et al. (1983). **c** Geometry of structures used for computations, drawn from the analog models. *L* Length crossed by a B-type surface (**b**) through the cryptodome ▶

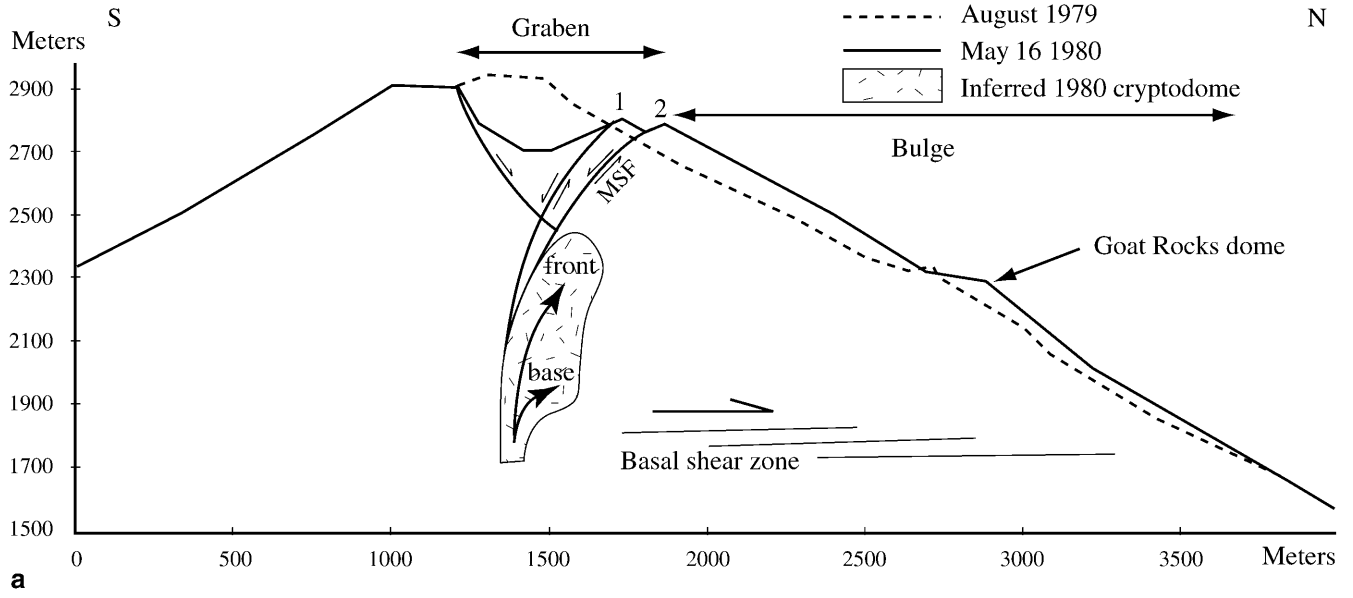
S
N
Meters
Graben
August 1979
May 16 1980
Inferred 1980 cryptodome
1
2
Bulge
MSF
front
base
Goat Rocks dome
Basal shear zone
2900
2700
2500
2300
2100
1900
1700
1500
0
500
1000
1500
2000
2500
3000
3500
Meters

a

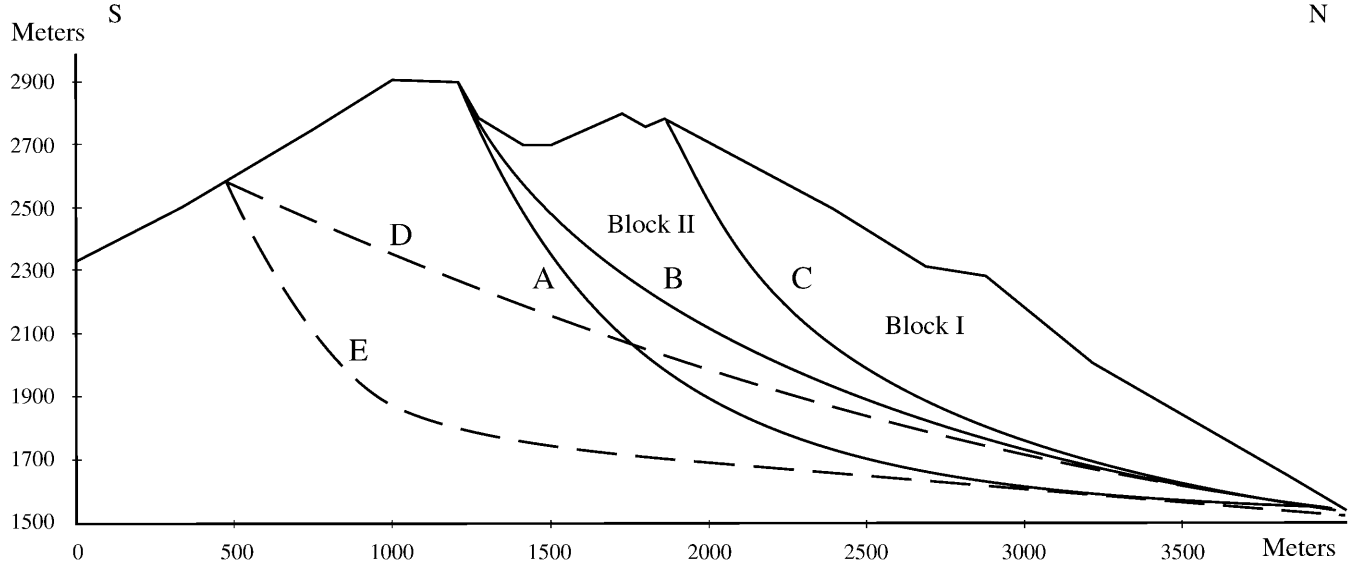
S
N
Meters
D
A
B
C
E
Block II
Block I
2900
2700
2500
2300
2100
1900
1700
1500
0
500
1000
1500
2000
2500
3000
3500
Meters

b

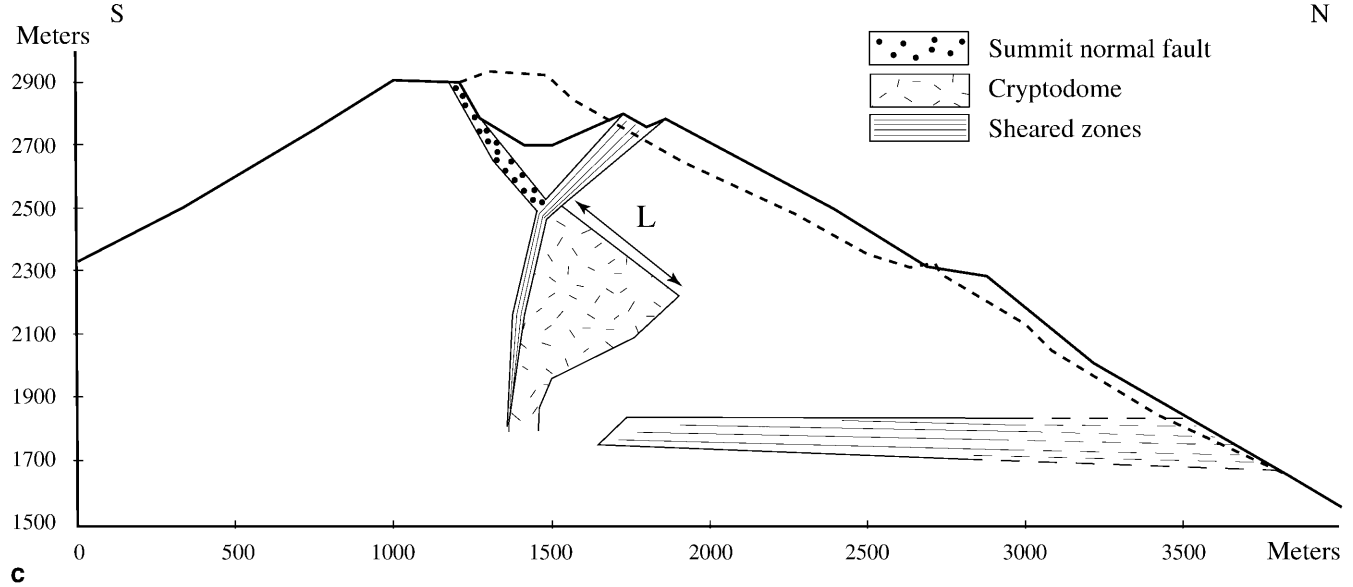
S
N
Meters
Summit normal fault
Cryptodome
Sheared zones
L
2900
2700
2500
2300
2100
1900
1700
1500
0
500
1000
1500
2000
2500
3000
3500
Meters

c

Table 1 Causes of volcano instability during cryptodome intrusion

1. Cryptodome-induced structural deformation, as revealed by analog models (Donnadieu and Merle 1998)
(a) Large magmatic body, hot and viscous, thus mechanically weaker than the edifice
(b) Major shear fault (MSF) separating a graben structure in the summit area and a large-scale lateral bulge (Fig. 1a); the MSF propagates upward from one side of the magmatic intrusion to the surface on the opposite flank to form the bulge crest
(c) Summit system of normal faults dipping outwards in graben region, and therefore prone to failure
(d) Shear zone developed at the base of the bulged flank; shearing may culminate ultimately with the formation of a surface thrust (Merle and Donnadieu 2000)
(e) Increased slope on the bulged flank
(f) Upturning of strata (planes with low shear strength) near the crest of the bulge
2. Processes induced by the magmatic activity
(a) Mechanically and thermally induced pore fluid pressures (Voight and Elsworth 1997)
(b) Shallow seismicity caused by edifice and basement fracturing in response to intrusion
(c) Weakening of the near-crater area by phreatic or phreatomagmatic explosions
3. Usual causes inherent to volcanic areas
(a) Edifice strength in terms of rock cohesion, angle of friction, fracturation and preexisting weak structures
(b) Hydrothermal alteration of large portions of the edifice
(c) Water table
(d) Tectonic earthquakes

and the weight of each slice in the landslide cross section.

Analysis is two-dimensional; that is, for a slope cross section (Fig. 1c). The condition for failure is Fs≤1.

Influence of material properties, pore pressure and seismicity

The shape of the failure surface is mostly influenced by the material intrinsic parameters, but can be controlled by earthquake-induced ground accelerations or guided by weak structures within the edifice. The next part of the paper deals with this latter aspect. In this part, we study the influence of rock properties and seismic loading on the stability of a structurally homogeneous edifice. Strength parameters, e.g., friction angle and cohesion, are poorly known on the scale of a volcanic edifice. Pore water pressure and seismic loading vary with time and position, and may be quite different from one volcano to another. These are the reasons why we investigate stability through a large range of input values. Computations are made with the pre-collapse topography of Mount St. Helens and the results are given for trial surface B (Fig. 1b) because it is of intermediate depth.

Effect of bulk density

The effect of a large range of rock density values (2,000–2,800 kg m^{-3}) on stability is tested for circle B for an average angle of friction of 40°. As displayed in Fig. 2a, Fs is insensitive to bulk density. Although gravity is a main driving force in destabilization, the range of possible densities have a minor effect on stability. The value of 2,400 kg m^{-3} used by Voight et al. (1983) is used in the additional computations.

Effect of cohesion

A range of cohesion (c) values over several orders of magnitude shows a distinct correlation to the factor of safety Fs (Fig. 2b). Variations of c up to 10^5 Pa have negligible influence on Fs, notably for slip-circles B and C taken from Voight et al. (1983) (Fig. 1b). Introducing a pore pressure, or decreasing the friction angle from 40 to 30°, changes Fs values but does not alter the basic trend. However, for $c>10^6$ Pa the effect of the cohesion becomes increasingly influential and inhibits rupture along circle B. For instance, an edifice with $c=5\times10^6$ Pa is stable, even with modest frictional strength, significant fluid pressure and strong seismicity ($\phi=30°$, $r_u=0.3$, $n=0.3$). Values $c>10^7$ Pa are those of intact crystalline rocks (Jaeger and Cook 1971). Schultz (1996) reported that the cohesion of a rock mass can be decreased by a factor of 10 compared with an intact sample because of fractures existing at a scale larger than the sample. In addition, a stratovolcano may be partly made of numerous pyroclastic layers and loose breccias, which offer little resistance to tensile or shear failure (Day 1996). These considerations suggest that the bulk cohesion of Mount St. Helens Volcano could not have much exceeded 10^6 Pa before failure. On the other hand, steep cliffs bounding the horseshoe-shaped crater nowadays attest that, locally, edifice cohesion is significant. Therefore it seems reasonable to consider a rock mass cohesion for Mount St. Helens in the range 10^5–10^6 Pa, when $\phi\approx40°$ and $r_u=0$–0.3 are assumed. This range is consistent with the maximum cohesion value of 6×10^5 Pa proposed by Voight et al. (1983) and with the value of 10^6 Pa used by Reid et al. (2000).

Effects of friction angle

Fs is sensitive to the internal angle of friction ϕ for various assumed sets of cohesion and pore pressure (Fig. 2c). When the fluid pressure effect is absent ($r_u=0$),

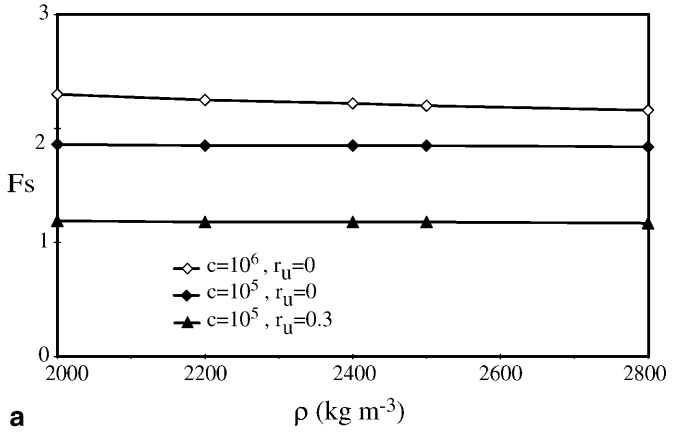

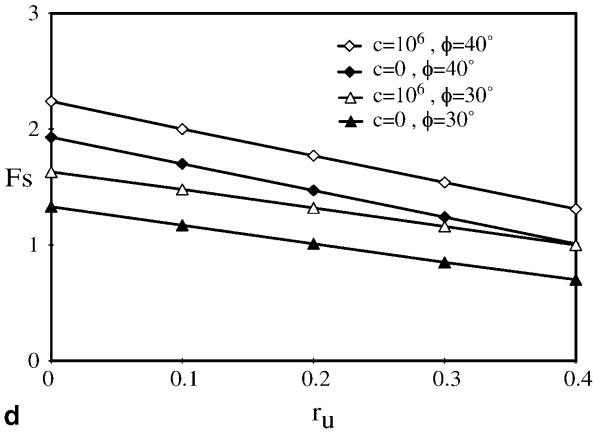

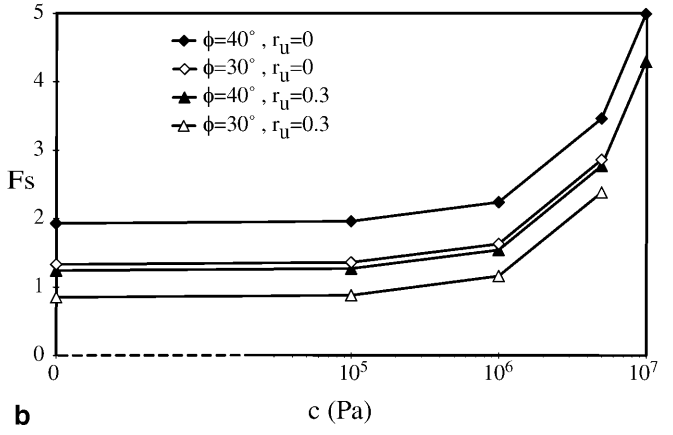

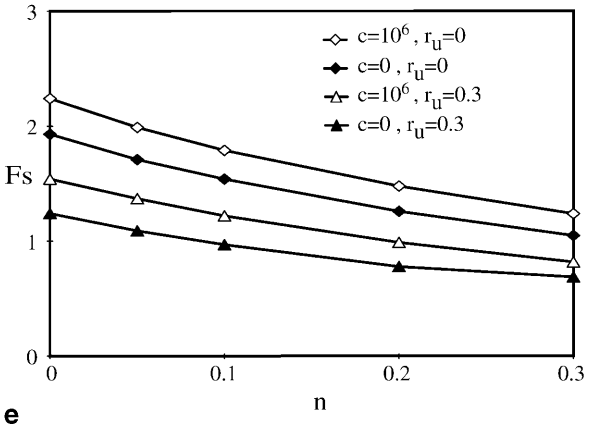

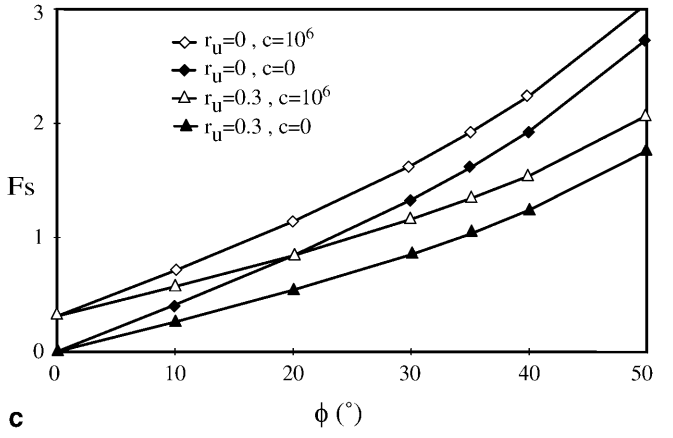

Fig. 2 **a** Influence of the bulk density ρ on Fs of circle *B* (Fig. 1b) for three conditions of cohesion c (Pa) and pore pressure (r_u); angle of friction ϕ=40° and seismic coefficient n=0. **b** Effect of the cohesion c in Pa (logarithmic scale) on the safety coefficient Fs for a *B*-type circle (Fig. 1b) and different values of friction angle ϕ and pore pressure r_u. Seismic coefficient n=0. Note change of scale between c=0 and c=10^5 Pa. **c** Influence of the friction angle ϕ on the safety coefficient of circle *B* (Fig. 1b) for two values of cohesion (c, in Pa) and pore fluid pressure (r_u). Seismic coefficient n=0. **d** Influence of pore pressure r_u on Fs of a *B*-type circle (Fig. 1b) for several values of cohesion (c, in Pa) and angle of friction (ϕ). Notice the correlation to the latter. **e** Consequence of a ground acceleration n in the horizontal direction on Fs of a *B*-type surface (Fig. 1b). n is believed to simulate the effects of an earthquake and is expressed as a fraction of gravity acceleration. Angle of friction ϕ=40° and two values of cohesion (c, in Pa) and pore fluid pressure (r_u) are tested

Fs is strongly dependent on ϕ. Thus, Fs increased from 1.61 to 1.93 as ϕ increased from 35 to 40°. With ϕ=45°, stability is achieved in almost every condition, including the case of strong seismicity (n=0.2). Pore fluid pressure (r_u=0.3 for instance) significantly reduces the influence of the friction angle, especially for high ϕ values. For ϕ=40°, Fs drops from 1.93 to 1.24 for r_u from 0 to 0.3, while for a theoretical ϕ=20°, Fs decreases only from 0.84 to 0.54 (Fig. 2c). The reason is because pore pressure acts on the friction component of strength, but not on the cohesion component.

From Fig. 2b, c it is possible to infer that ϕ should generally be greater than 30°, because otherwise a surface as deep as B would be below the limit equilibrium, even without seismic loading, in an edifice with c=10^5 Pa and r_u=0.3, possibly “ordinary” conditions for a stratovolcano (cf. Voight et al. 1983 for Mount St. Helens). Thus, at Mount St. Helens, it is likely that the rock-mass angle of friction was between 35 and 45°. This estimation is in good agreement with the value of 40° obtained by Voight et al. (1981) from engineering trials on materials from the debris avalanche.

Table 2 Fs values for surfaces at Mount St. Helens and Bezymianny Volcanoes with varied conditions of pore fluid pressure (r_u) and seismic coefficient (n)

	Mount St. Helens					Bezymianny				
	A	B	C	D	E	A2	B2	C2	D2	E2
r_u=0, n=0	2.34	1.96	1.85	2.95	4.07	3.19	2.13	1.55	2.69	4.05
r_u=0.3, n=0	1.55	1.27	1.18	2	2.79	2.18	1.40	0.96	1.82	2.76
r_u=0, n=0.2	1.56	1.28	1.26	1.67	2.29	1.95	1.33	1.03	1.56	2.30
r_u=0.3, n=0.2	1.03	0.80	0.77	1.1	1.52	1.31	0.84	0.60	1.09	1.56

Sliding surfaces are indicated in Fig. 1c for Mount St. Helens and in Fig. 3 for Bezymianny Volcano. The edifice has an angle of friction ϕ=40° and a cohesion c=10^5 Pa

Effects of pore-fluid pressure

Values of r_u typically range from 0 ("dry" conditions) to 0.4. A value of r_u>0.4 would correspond to artesian conditions, which we think are unlikely at Mount St. Helens since it implies a piezometric level well above the ground surface. Pore-fluid pressure reduces normal stresses on a potential failure surface, reducing its shear resistance (Hubbert and Rubey 1959). Therefore, increasing r_u weakens the edifice (Fig. 2d). Thus r_u=0.3 causes the Fs of circle B to decrease by 30% compared with dry conditions in an edifice with c=10^6 Pa and ϕ=40°. The relative influence of r_u on Fs becomes stronger when the angle of friction is higher, as seen from the slopes on Fig. 2d, which are steeper (×1.5) for conditions with ϕ=40° than for those with ϕ=30°. Voight and Elsworth (1997) suggested that intrusion-related mechanical and thermal straining of the rock–fluid medium, resulting in excess pore pressure, could initiate and sustain massive volcano collapse. Many processes related to volcanic environment can increase pore fluid pressure, as discussed by Day (1996). Earthquake-induced shaking and fluid pressure processes may act concurrently.

Effects of seismicity

The assumption that the seismic coefficient n could have exceeded 0.2 times the gravitational acceleration during the earthquake that presumably triggered the Mount St. Helens failure is not unrealistic (Voight et al. 1983). Computations show that horizontal ground accelerations have a stronger influence than vertical accelerations on the Fs values of surfaces A, B, and C. Therefore, we hereafter consider only the effects of horizontal ground accelerations. Figure 2e suggests that a ground acceleration of 0.1 *g* reduces Fs by more than 20%, and of 0.3 *g* by more than 45%, for the various conditions. The effect of ground acceleration is not particularly sensitive to the cohesion (c≤10^6 Pa) and pore pressure (r_u=0.3) assumed. Curves associated with r_u=0 indicate that, under dry conditions, a horizontal acceleration of about 0.3 *g* does not succeed in generating a failure on a B-type surface, i.e., Fs>1, in an edifice with c=10^6 Pa (Fig. 2e). Nor could failure occur along A and C surfaces in dry conditions with n=0.2 and c=10^5 Pa (Table 2). If r_u=0.3, however, a ground acceleration of 0.1–0.2 *g* leads to Fs<1 on surfaces B and C and marginal stability of the deeper surface A (Table 2). Because seismicity is very common in volcanic areas, its strong influence makes it an important trigger for slope destabilization.

Shape of failure surface in a homogeneous edifice

When the cone is modeled as a homogeneous mass, computations show that the larger the cohesion, the deeper the critical circle of failure (the circle representing the minimum Fs value). A B-type critical circle is obtained for ϕ=40° and c=5×10^6 Pa on the Mount St. Helens profile. Under these specific conditions however, Fs remains high and prevents failure (Fs>2.7, r_u=0–0.3; Fig. 2b). For lower, and probably more realistic, cohesion values (10^5<c<10^6 Pa), the critical surface (minimum Fs) tends to be shallower, with higher curvature radius. Voight et al. (1983) found a critical circle of type C for ϕ=40°, c=10^6 Pa and r_u=0.3 with Fs=1.52, although this cohesion is higher than the rock-mass value suggested by these authors for Mount St. Helens. Therefore, unlike B-type surfaces, surfaces C (Mount St. Helens) or C2 (Bezymianny) are critical for c=10^6 Pa and can be decreased to less than unity by high pore fluid pressure combined with severe ground acceleration (Table 2).

Computations generally show that, for a cone containing no weak structures, the deeper the potential failure surface, the higher the Fs value. In particular, deep concave-shaped surfaces can have high Fs values because their lower parts of shallow dip offer considerable resistance to sliding. For instance, surfaces A (Fig. 1b) or A2 (Fig. 3) are more stable than their counterpart B or B2 surfaces starting from the same place in the cone (Table 2). Thus, they do not correspond to critical surfaces. Under these conditions, slope oversteepening or minor seismic ground shaking should favor shallow landslides and rock falls. These were observed at Mount St. Helens and Bezymianny Volcanoes prior to their collapse.

Deep-seated avalanche calderas

Siebert (1984) noticed that many volcanic sector collapse scars are deep, encompassing the summit and conduit, and make a marked angle between the internal wall

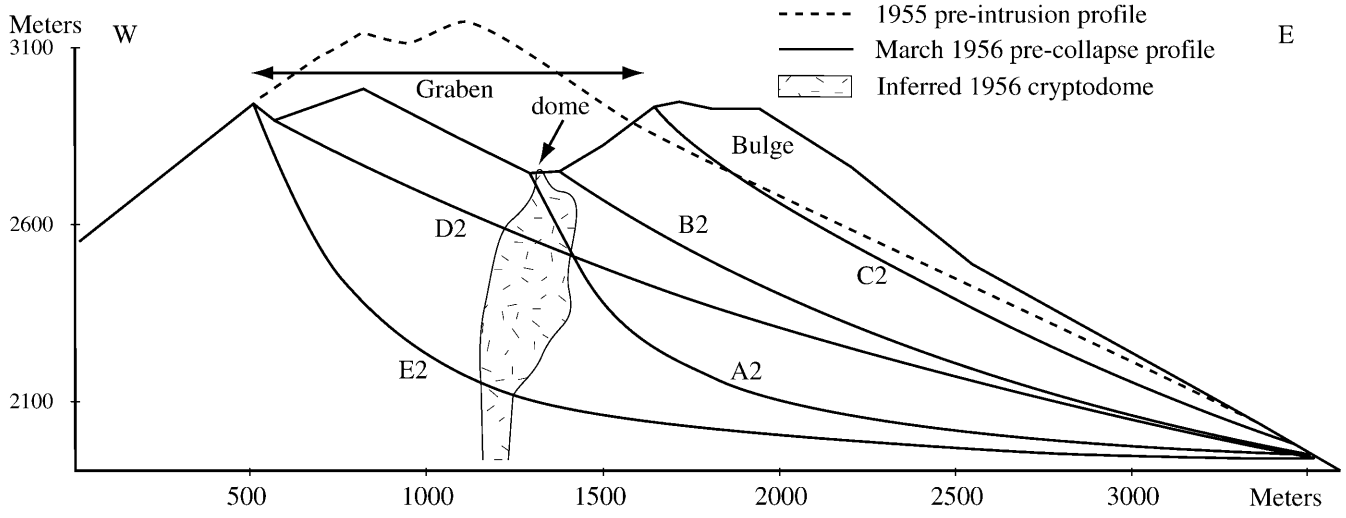

Fig. 3 Trial surfaces tested in the case of Bezymianny Volcano. The outline is taken from a photograph of Gorshkov (1959). Surface E2 approximately corresponds to the post-collapse scar profile

and the floor that dips gently outwards. The sliding surfaces of non-volcanic landslides are usually more superficial and relatively planar. Siebert ascribes these differences chiefly to the existence of pyroclastic and altered materials at the volcano's summit and to the explosive activity that often accompanies major collapses. The results of the first part of our study account for the typical non-volcanic landslide morphology because the data suggest that shallow surfaces are less stable in a homogeneous edifice with cohesion of ~10^5–10^6 Pa. The reason why volcanic debris avalanches are often deeply rooted is less obvious.

We tested the hypothesis that these deep-seated sector-collapse scars could be the result of a single slide in a homogeneous edifice. Stability computations show that deep-seated surfaces have very high Fs values. Shallower circles always display a greater instability. For a homogeneous cone, deep surfaces E (Fig. 1b) or E2 (Fig. 3) are associated with Fs>4 for ϕ=40° and c=10^5 Pa (Table 2). Although it is possible to define planar surfaces with lower Fs that might fail with severe seismic and pore pressure conditions (e.g., surfaces D or D2; Figs. 1b and 3), such planar surfaces could not alone explain the depth of typical volcanic sector-collapse scars.

We also simulated a heterogeneous edifice with a large central core characterized by weak properties (ϕ=20°, c=0, r_u=0.3), taken as representative of hydrothermally altered rock. In this case, Fs>2 for surface E. If these extremely weak properties are assigned to the whole length of surfaces E or E2 that represent typical avalanche caldera profiles, then Fs can approach unity. It might represent the specific case in which fluid circulation (and alteration) is restricted to zones that lie along the whole failure surface, as governed by pre-existing structural discontinuities, or the contact between basement rocks and the volcanic pile (Lopez and Williams 1993). Such a case may rarely exist. In contrast, if the hydrothermal alteration is widespread, then it might not support the 30° outer slope of the cone. Such a spreading mechanism has been proposed to account for morphologic features of Casita Volcano, Nicaragua (van Wyk de Vries et al. 2000).

Although we cannot preclude that particularly strong seismic conditions could lead to the typical morphology of deep avalanche calderas, it is unlikely that steep internal walls and a flat floor could generally form through a unique single slide. A combination of strong seismicity and pore pressure conditions would lead again to a relatively planar landslide because Fs associated with this kind of surface is lower.

Following Voight et al. (1983), Siebert et al. (1987) and Voight and Elsworth (1997), we therefore suggest that multiple retrogressive slides occur in most cases to generate such a resulting morphology, as a consequence of one or several specific conditions existing in volcanic environments: hydrothermal alteration, presence of a magmatic body, or explosive mechanisms with cohesion destroyed, and high pore fluid pressures in magmatic or hydrothermal systems. Accordingly, we hereafter consider the influence of a cryptodome intrusion on potential slip surfaces and then on the formation of volcanic avalanche calderas.

Effects of deformation produced by a cryptodome

Topographic changes

If the emplacement of a cryptodome is asymmetric and oriented toward one flank, two major topographic features arise (Donnadieu and Merle 1998): (1) a summit graben elongated perpendicular to the displacement of the flank, which can be hundreds of meters wide and several kilometers long; (2) a bulge outboard of the graben, corresponding to the more or less horizontal translation of the flank (~150 m in the case of Mount St. Helens). Such topographic changes were recorded at

Table 3 Fs values of a B-type surface (Fig. 1b) for Mount St. Helens topography before the cryptodome intrusion in 1979 and before the eruption of 18 May 1980, under various conditions of friction angle (ϕ), cohesion (c) and pore pressure (r_u). No internal structure is taken into account, only topography is considered. Seismic coefficient n=0

r_u	c (Pa)	Topography 1979		Topography 05/18/1980	
		ϕ=30°	ϕ=40°	ϕ=30°	ϕ=40°
0	0	1.26	1.82	1.33	1.93
	10^5	1.3	1.86	1.36	1.96
0.3	0	0.8	1.16	0.85	1.24
	10^5	0.84	1.2	0.88	1.27

Mount St. Helens from photographs between August 1979 (prior to the beginning of the deformation) and 16 May 1980 (Moore and Albee 1981; Voight et al. 1981), and similar deformation was documented at Bezymianny Volcano prior to the failure (Gorshkov 1959).

Reid et al. (2000) calculated that deformation at Mount St. Helens was responsible for a decrease of Fs by 3% over the undeformed edifice. Their three-dimensional method resulted in a minimum Fs of about one in the bulge area and an associated potential failure volume of ~1.1 km^3 with c=10^6 Pa, r_u=0.3 and n=0.2. They recognized, however, that small uncertainties in Fs could lead to large uncertainties in potential failure volume. The location and volume uncertainty may fit that of slip surface C. However these conditions alone do not account for the failure of block II along a deeper failure surface of B type. Because block I and block II were seen moving simultaneously, we suggest that B was the critical surface and was at marginal stability prior to the collapse, reflecting the existence of cryptodome-generated weakening structures. According to our calculations, the topographic changes are responsible for Fs increases along fixed circle B by 5–6%, no matter what ϕ and r_u values are used (Table 3). Thus, the removal of mass from the crater and the displacement of the center of gravity of the north flank downslope contributed to stabilizing surface B, whereas the slope increase lowered Fs on potential slip surface C. As the slope became more pronounced, it promoted superficial failures on the bulge, forming small avalanches and rock falls during earthquakes.

We also modeled the static stability of the transient topography at the beginning of the collapse of block I. For an arbitrary transient scarp height of 500 m, the displacement of block I causes Fs of surface B to rise from 1.96 to 2.01; that is, block I displacement makes block II more stable. Therefore, the displacement of the mass of block I alone cannot explain the failure of block II. Nevertheless, shaking caused by the triggering earthquake, added to the vibration originating from the motion and dislocation of block I, may have contributed to detachment of the second block. Voight et al. (1981) and Lipman et al. (1981) suggested that the northern flank had not reached its limit equilibrium earlier because of (1) the lack of ground-deformation acceleration of survey points, which is often recorded just before landslides and, sometimes, eruptions (Swanson et al. 1983; Voight 1988; Voight and Cornelius 1991; Murray et al. 1994); and (2) the powerful earthquake that likely triggered the failure (Voight et al. 1981; Kanamori et al. 1984; see discussion). Besides, analog models of intrusion often display a thrust, which appears at the surface at the base of the bulge because of large lateral displacement of the flank (Merle and Donnadieu 2000; Fig. 1c). No signs of a thrust fault were detected at Mount St. Helens prior to the 18 May 1980 eruption, suggesting that the intrusion could have developed further if no earthquake had triggered the failure. Also, at least four other older domes extruded at Mount St. Helens without a major failure at the summit and on the northern side (Crandell and Mullineaux 1978; Hoblitt et al. 1980).

Summit structures: major shear fault and normal faults

The shear zone that propagates from one side of the magmatic body to the fractured crest of the bulge may contain several faults (major shear faults or MSF of Donnadieu and Merle 1998; Fig. 1a). This zone is represented by an inward-dipping layer with variable properties of angle of friction and cohesion (Fig. 1c). Whatever the characteristics chosen, all potential slip surfaces intersecting this zone receive no significant effect on Fs because it forms too small a fraction of their surface. Therefore, although the MSF is the major structural element controlling the emplacement of a cryptodome, it does not directly affect edifice stability.

As magma is guided obliquely by the MSF, the flank is displaced outward and a series of normal step faults are generated very early to accommodate the summit extension. These normal faults join the MSF at shallow depth (Fig. 1a). As they experience episodic motion (>2 months at Mount St. Helens), cohesion along the fault system is presumably reduced. The main normal fault is symbolized by a thin, cohesionless layer dipping at 60° outward (Fig. 1c). Computations show that this structure, because of its limited dimensions, has only limited effect on the Fs of surfaces going through it, irrespective of its properties and the shape of the surface. For example, theoretical considerations for surface B give Fs=1.93 for ϕ_{fault}=22°, and Fs=1.92 for ϕ_{fault}=1°, with the rest of the edifice having c=10^5 Pa, ϕ=40°, r_u=0 and n=0. Shallower surfaces are a priori more unstable than surfaces passing through this zone. There are three possibilities for initiating failure along this zone (B): (1) powerful seismic accelerations, which would increase sufficiently the driving moments to trigger failure of a large portion of the edifice back to this mechanically-weak zone; (2) the presence of another weak structure that diminishes the resisting moments; or (3) a combination of both. The second hypothesis is tested below.

Magma body

Physical models show analog magma intruding upward along the MSF. As a general result, the head of the intrusion could be cut by any landslide running at a significant depth. In the case of Mount St. Helens, the front of the magma body seemed to be cut by the second slide (Voight et al. 1981). The dacite cryptodome was at magmatic temperatures of ~900 °C, with a phenocryst content of 30 vol%, a vesicularity of 36 vol% and a bulk water content of only 0.6 wt%, corresponding to a highly viscous, nearly solid, state (Eichelberger and Hayes 1982; Alidibirov et al. 1997). Therefore, the magma body represented a mechanical weakness within the edifice. For example, Heuze (1983) found experimentally a dramatic decrease of c and ϕ in granitic rocks as a function of temperature, by more than 90% at 900 °C. Although the cohesion and angle of friction of the Mount St. Helens hot dacite (c_{crypt} and ϕ_{crypt}) have not been measured, we anticipate similarly that they were much reduced because of the magmatic temperature and high vesicularity. In our model we do not try to reproduce faithfully the behavior of a viscous fluid undergoing rapid mechanical stresses, but simply to model a zone of low strength compared with the rest of the cone. For this reason, a large range of values of ϕ_{crypt} and c_{crypt} is tested for the cryptodome within an edifice with ϕ=40° and c=10^5 Pa. Over the physical parameters ascribed to this zone, the most important element is the length (or 3-D a surface) cut by the failure surface. It implies that the cryptodome may take on a different shape than that drawn in Fig. 1c.

Introducing a zone with physical properties weaker than those of the edifice has a twofold effect on a B-type circle cutting its front: (1) Fs of this circle is markedly lowered; and (2) Fs is at minimum for this circle: it is the critical circle, compared to overlying failure surfaces. Thus the presence of a cryptodome at this position in the edifice could help explain why failure of block II occurred on a relatively deep-seated surface. Table 4 gives Fs values for a surface passing through the cryptodome with a cutting length L (Fig. 1c). The critical failure surface is of type B; Fs is a minimum when the cutting length is equal to L/2 or larger; that is, even for a cryptodome with a narrow front. Computations also show that the edifice containing such a magma body can be destabilized if it experiences a moderate horizontal acceleration about 0.25 *g*, without the need for additional pore pressure or weak structures. When the cutting length is less than L/2, Fs is naturally higher, and lower values are found for more superficial planar surfaces. In contrast, when the cryptodome length cut by the critical surface is 2L, Fs is seriously diminished and the stability is rendered extremely sensitive to pore pressure and seismicity conditions. Only the general trends arising from the presence of a cryptodome are emphasized here because the three-dimensional effect is not taken into account.

Table 4 Fs values associated with a B-type surface cutting through the cryptodome over a length L, L/2 or 2L (Fig. 1c). A mechanically weak body with two possible values of angle of friction ϕ and cohesion 0≤c≤10^4 Pa is tested. Note results are very close for lower and upper values of c. The edifice has ϕ=40° and c=10^5 Pa. The effect of an earthquake-induced horizontal ground acceleration (n) is indicated for an intrusion of average size

Cryptodome c=0–10^4 Pa	ϕ=10°	ϕ=20°
L/2	1.85	1.89
L	1.72	1.80
L×2	1.49	1.65
L, n=0.25	1.03	1.08

Basal shear zone underlying the bulge

Analog models of intrusion display a lateral intrusion of the "magma" at the base of the bulge and eventually display a thrust that appears at the base of the bulge (Fig. 1a). This and the overall horizontal displacements of the Mount St. Helens bulge suggest that a shear zone propagated from the base of the cryptodome toward the outer cone surface because of the magma pushing out the flank. Voight (1988) also considered the possibility of a slope pushed out on its side like a "compression test", leading to rupture after a critical strain is reached on a 2-km-long subhorizontal plane underlying the north flank. The shear-zone geometry used for our calculations is shown in Fig. 1c. Again, the important parameter for analysis is the length of the intersection between the shear zone and the potential failure surface (~800 m for surface B), not the shape of the shear zone. The angle of friction and the cohesion of the shear zone should approach that of a fault zone. As these may vary, we took 10°≤ϕ_{shear}≤30° and 0≤c_{shear}≤10^5 Pa because the cohesive strength was presumably much destroyed because of earlier movement. In all cases, Fs is lowered by 7 to 21%, compared with the case in which a shear structure is absent: thus, Fs=1.69 for ϕ_{shear}=22°, c_{shear}=0 instead of Fs=1.96. Besides, there is always a critical surface of type B, merging with the deep shear zone downslope. Also, the presence of such a deep shear zone, in addition to intense fracturing at the crest of the bulge and slope oversteepening caused by the magmatic push, could also explain failure along surface C at Mount St. Helens under seismic shaking.

Combined effects of cryptodome structures

The emplacement of a cryptodome generates all the structures investigated, leading locally to a very low Fs, with failure clearly localized along a deep critical surface of type B. With the average mechanical properties assumed in Table 5 for both the edifice and the structures produced by the cryptodome, computations give Fs=1.53, without any pore pressure or seismicity, compared with Fs=1.96 without cryptodome structures (Table 2) under the same conditions. Thus, the growth of

Table 5 Combined effect of the structures generated by a cryptodome on Fs associated with critical failure surface B at Mount St. Helens (Fig. 1b). Average mechanical properties of all structures are considered. Failure may occur (Fs≤1) if r_u=0.3 or if n=0.2

	ϕ (°)	c (Pa)	r_u=0 n=0	r_u=0 n=0.2	r_u=0.3 n=0
Edifice	40	10^5			
Graben and craters	40	10^5			
Normal fault	25	0	Fs=1.53	Fs=1	Fs=0.99
Cryptodome	20	10^4			
Basal shear zone	22	0			

a cryptodome within the volcano reduces stability and renders it more sensitive to triggering mechanisms. Nevertheless, it is possible that intrusions can sometimes reach the surface without catastrophic destabilization (e.g., Goat Rocks at Mount St. Helens). For the assumptions cited above, a horizontal acceleration of 0.2 *g* alone is able to cause failure of surface B (Fs=1, Table 5). Likewise, failure can be triggered without seismicity if during the growth of the intrusion significant pore pressure (r_u=0.3) develops in the interior of the edifice (Table 5). If both seismicity and pore pressure are present, rupture may occur with even lower values of r_u and n. Also, if unfavorable conditions with r_u=0.3 and n=0.2 are combined, edifices with a larger cohesion (10^6 Pa or slightly higher) could be destabilized along a B-type deep surface because of cryptodome-induced deformation.

A deep-seated surface (E or D) cutting through the cryptodome and its basal shear zone (Fig. 1c) would have Fs>>2, even with structures characterized by a very low angle of friction (10°) and no cohesion. Thus, it is likely that deep debris avalanche scars do not result from a single slide, even when cryptodome emplacement generates weakening structures deep within the volcano.

Discussion and conclusions

Stability of Mount St. Helens prior to 18 May 1980

Intrusion of a cryptodome into the upper part of a volcanic edifice decreases its stability because of the lower shear strength of the magmatic body itself and associated weakening structures, including outward-dipping normal faults bounding a summit graben, bulging of the destabilized flank, and a subhorizontal shear zone at the base of the bulge. Our results suggest that these structural deformations contribute directly to localized failure along a critical surface with low Fs deep within the interior of the edifice. This critical surface, with Fs reduced by as much as 25–30%, is then very sensitive to the variations of stability conditions, particularly to pore pressure and seismicity, and may lead to catastrophic failure of a large volume of the edifice flank (e.g., for r_u=0.3 or n=0.2). In the case of Mount St. Helens, the critical surface fits the deep sliding surface of block II (surface B).

Voight et al. (1983) showed that Fs associated with surfaces B or C at Mount St. Helens could be decreased to less than unity when significant pore pressure and earthquake-induced ground accelerations were combined. We find however that, in the general case of a homogeneous edifice, the critical surface (minimum Fs) is shallow and cannot fit B or C type surfaces when 10^5<c<10^6 Pa. Several factors could account for a critical surface of depth comparable to C: (1) a rock mass cohesion of ~10^6 Pa; (2) the basal shear zone generated by the cryptodome growth, which may have lowered the stability of surface C and located the lower end of the slip surface; and (3) particular seismic conditions might have influenced the depth of the critical surface, as the critical surface during an earthquake is not necessarily the same as that without seismicity. In all three cases, however, failure of block I along surface C required a combination of unfavorable conditions of pore fluid pressure and seismicity (r_u≥0.3 and n≥0.2), as previously suggested by Voight et al. (1983). We agree with these authors that failure occurred in a material with an angle of friction around 40°, rock mass cohesion of 10^5<c<10^6 Pa (but more likely in the upper range), and significant water pore pressure.

On 18 May 1980, E–W trending fractures appeared soon after the magnitude 5.2 earthquake on the crest of the bulge (Voight et al. 1981). They were the first sign of the detachment of slide block I along a newly formed rupture surface of type C. The bulge crest was sheared and crushed owing to large displacements along the inward-dipping faults resulting from cryptodome indentation. This may have helped C become a critical surface, although there is no clear evidence for it. Also, shearing that occurred at the base of the bulge, owing to the lateral push of the magma, may possibly have contributed to the failure of surface C, but more likely to the failure of B, which was deeper. The detachment of the second block along a B-type surface occurred simultaneously and clearly used the largest normal fault bounding the graben to the south. Our results suggest that the shape of slide surface B has been guided at depth by the cryptodome front, and also its basal shear zone. For these reasons, we believe that B became a critical surface, and that it was on the verge of failure even before the triggering earthquake. It is likely that the Mount St. Helens cryptodome and its basal shear zone were not quite developed enough to generate a critical surface during the preceding magnitude 5 earthquakes of 8 and 12 May, although sudden shifts of the slope occurred at this time (Voight et al. 1983). Part of the seismic activity might well be the consequence of the propagation of surface B. The cryptodome structures were probably weakened by these events, allowing the 18 May earthquake, of comparable magnitude (Endo et al. 1981), to trigger the catastrophic failure. Thus, the 18 May earthquake caused the sliding of surface B, which had reached marginal stability owing to the development of the cryptodome structures, and triggered the failure of a newly formed surface of type C, helped by the slope increase. On the basis of

our limit-equilibrium analysis, we believe that the earthquake was the trigger of the Mount St. Helens rockslide avalanche, challenging Kanamori et al. (1984) interpretation from seismic body waves that the earthquake represents the onset of the landslide. Had no earthquake occurred, surface B might have failed alone when cryptodome structures had become sufficiently developed or pore fluid pressure had become too high to support the northern flank.

Stability of Bezymianny Volcano

In the case of Bezymianny Volcano, the duration and magnitude of deformation, as well as the presence of a flat lava dome in the crater prior to failure and strombolian eruptions, suggest that the intrusion was well developed. A very similar scenario to Mount St. Helens certainly occurred following an earthquake (Gorshkov 1959) and involved several failure surfaces (Siebert et al. 1987; Voight and Elsworth 1997). Possible slides along arbitrary surfaces of type C2 then B2 or A2 (Fig. 3), first depressurized the magmatic system, allowing the emission of a lateral blast. If weakening cryptodome structures are not considered, then B2-type surfaces cannot represent critical surfaces. Also, pore pressure and seismicity conditions stronger than at Mount St. Helens might have been required to reach the rupture threshold because the stability of surfaces A2 and B2 is significantly higher than equivalent surfaces at Mount St. Helens. In both cases, had no earthquake occurred, the cryptodomes would have grown more, producing rock falls and minor avalanches, until sufficient strength loss along a surface of type B permitted sliding of the rock mass above.

Several domes known on the flanks of Mount St. Helens, like Goat Rocks, could represent the non-catastrophic outcome of the process clarified experimentally by Donnadieu and Merle (1998). Other cryptodome deformations have been witnessed at Usu-Shinzan (Katsui et al. 1985) and Showa-Shinzan (Minakami et al. 1951) Volcanoes in Japan. They did not culminate in a landslide associated with a paroxysmal eruption like at Mount St. Helens or Bezymianny because they were emplaced beneath relatively flat ground.

Formation of deep-seated avalanche calderas

Our computations show that the typical scar profiles of deep-seated avalanche calderas, which display a sharply dipping headscarp and a relatively flat floor, cannot generally be created by a single slide neither in a mechanically homogeneous edifice, nor in an edifice weakened by cryptodome-induced structures. This result corroborates the idea of Voight et al. (1983), Siebert et al. (1987) and Voight and Elsworth (1997) that they result from multiple retrogressive slides, sometimes aided by powerful explosions of magmatic and hydrothermal fluids at high pressure, and fluidization of cohesionless debris. For Mount St. Helens, we show that the cryptodome weakening structures localize a second concomitant critical surface of type B, deeper than C, and may therefore account for retrogressive slides. Therefore, cryptodome intrusions appear to be one possible cause for the formation of deep-seated avalanche calderas. Conversely, retrogressive slides do not necessarily imply the emplacement of a cryptodome.

Acknowledgements Philippe Labazuy and Benjamin van Wyk de Vries supplied helpful comments of an early version of the manuscript. We thank Andrea Borgia and Barry Voight for thoughtful reviews of the paper. This research work has been funded by the PNRN program of the French CNRS.

References

Alidibirov M, Dingwell DB, Stevenson RJ, Hess K-U, Webb SL, Zinke J (1997) Physical properties of the 1980 Mount St. Helens cryptodome magma. Bull Volcanol 59:103–111

Belousov AB, Bogoyavlenskaya GE (1988) Debris avalanche of the 1956 Bezymianny eruption. Proc Kagoshima Int Conf on Volcanoes, pp 460–462

Bishop AW (1955) The use of slip circles in the stability analysis of slopes. Géotechnique 5:7–17

Boudon G, Semet MP, Vincent PM (1984) Flank failure-directed blast at Soufrière, Guadeloupe, F.W.I.: a 3000 yr-old Mt St Helens? Geology 12:350–353

Crandell DR, Mullineaux DR (1978) Potential hazards from future eruptions of Mount St. Helens volcano, Washington. US Geol Surv Bull 1383-C

Day SJ (1996) Hydrothermal pore fluid pressure and the stability of porous, permeable volcanoes. In: McGuire WJ, Jones AP, Neuberg J, (eds) Volcano instability on the Earth and other planets. Geol Soc Spec Publ 110:77–93

Donnadieu F, Merle O (1998) Experiments on the indentation process during cryptodome intrusions: new insights into Mount St. Helens deformation. Geology 26:79–82

Eichelberger JC, Hayes DB (1982) Magmatic model for the Mount St. Helens blast of May 18, 1980. J Geophys Res 87: 7727–7738

Endo ET, Malone SD, Noson LL, Weaver CS (1981) Locations, magnitudes, and statistics of the March 20–May 18 earthquake sequence. In: Lipman PW, Mullineaux DR (eds) The 1980 eruptions of Mount St. Helens, Washington. US Geol Surv Prof Pap 1250:93–107

Gorshkov GS (1959) Gigantic eruption of the volcano Bezymianny. Bull Volcanol 20:77–109

Heuze FE (1983) High temperature mechanical, physical and thermal properties of granitic rocks – a review. Int J Rock Mech Min Sci 20:3–10

Hoblitt RP, Crandell DR, Mullineaux DR (1980) Mount St Helens eruptive behavior during the past 1,500 yr. Geology 8: 555–559

Hubbert MK, Rubey WW (1959) Role of fluid pressure in mechanics of overthrust faulting, I. Mechanics of fluid-filled porous solids and its application to overthrust faulting. Geol Soc Am Bull 48:115–166

Jaeger JC, Cook NGW (1971) Fundamentals of rock mechanics. Chapman and Hall, London

Jordan R, Kieffer HH (1981) Topographic changes at Mount St. Helens : large-scale photogrammetry and digital terrain models. In: Lipman PW, Mullineaux DR (eds) The 1980 eruptions of Mount St. Helens, Washington. US Geol Surv Prof Pap 1250:135–141

Kanamori H, Given JW, Lay T (1984) Analysis of seismic body waves excited by the Mount St. Helens eruption of May 18, 1980. J Geophys Res 89:1856–1866

Katsui Y, Komuro H, Uda T (1985) Development of faults and growth of Usu-Shinzan cryptodome in 1977–1982 at Usu volcano, north Japan. J Fac Sci Hokkaido Univ, Ser IV 21:339–362

Lipman PW, Moore JG, Swanson DA (1981) Bulging of the north flank before the May 18 eruption – Geodetic data. In: Lipman PW, Mullineaux DR (eds) The 1980 eruptions of Mount St. Helens, Washington. US Geol Surv Prof Pap 1250:143–155

Lopez DL, Williams SN (1993) Catastrophic volcanic collapse; relation to hydrothermal processes. Science 260:1794–1796

Merle O, Donnadieu F (2000) Indentation of volcanic edifices by the ascending magma. Geol Soc Lond Spec Publ 174:43–53

Minakami T, Ishikawa T, Yagi K (1951) The 1944 eruption of volcano Usu in Hokkaido, Japan. Bull Volcanol 11:45–157

Moore JG, Albee WC (1981) Topographic and structural changes, March–July 1980 – photogrammetric data. In: Lipman PW, Mullineaux DR (eds) The 1980 eruptions of Mount St. Helens, Washington. US Geol Surv Prof Pap 1250:123–134

Murray JB, Voight B, Glot J-P (1994) Slope movement crisis on the east flank of Mt. Etna volcano: models for eruption triggering and forecasting. Eng Geol 38:245–259

Paul A, Gratier J-P, Boudon J (1987) A numerical model for simulating deformation of Mount St. Helens volcano. J Geophys Res 92:10299–10312

Reid ME, Christian SB, Brien DL (2000) Gravitational stability of three-dimensional stratovolcano edifices. J Geophys Res 105: 6043–6056

Schultz RA (1996) Relative scale and the strength and deformability of rock masses. J Struct Geol 18:1139–1149

Siebert L (1984) Large volcanic debris avalanches: characteristics of the source areas, deposits and associated eruptions. J Volcanol Geotherm Res 22:163–187

Siebert L (1996) Hazards of large volcanic debris avalanches and associated eruptive phenomena. In: Scarpa R, Tilling RI (eds) Monitoring and mitigation of volcano hazards. Springer, Berlin Heidelberg New York pp 541–572

Siebert L, Glicken H, Ui T (1987) Volcanic hazards from Bezymianny- and Banda-type eruptions. Bull Volcanol 49:435–459

Siebert L, Begét JE, Glicken H (1995) The 1883 and late-prehistoric eruptions of Augustine volcano, Alaska. J Volcanol Geotherm Res 66:367–395

Swanson DA, Casadevall TJ, Dzurisin D, Malone SD, Newhall CJ, Weaver CS (1983) Predicting eruptions at Mount St. Helens, June 1980 through December 1982. Science 221: 1369–1376

van Wyk de Vries B, Francis PW (1997) Catastrophic collapse at stratovolcanoes induced by slow volcano spreading. Nature 387:387–390

van Wyk de Vries B, Kerle N, Petley D (2000) Sector collapse forming at Casita volcano, Nicaragua. Geology 28:167–170

Voight B (1988) A method for the prediction of volcanic eruption. Nature 332:125–130

Voight B, Cornelius RR (1991) Prospects for eruption prediction in near real-time. Nature 332:125–130

Voight B, Elsworth D (1997) Failure of volcano slopes. Géotechnique 47:1–31

Voight B, Sousa J (1994) Lessons from Ontake-san: a comparative analysis of debris avalanche dynamics. Eng Geol 38:261–297

Voight B, Glicken H, Janda RJ, Douglass PM (1981) Catastrophic rockslide avalanche of May 18. In: Lipman PW, Mullineaux DR (eds) The 1980 eruptions of Mount St. Helens, Washington. US Geol Surv Prof Paper 1250:347–377

Voight B, Janda RJ, Glicken H, Douglass PM (1983) Nature and mechanics of the Mount St. Helens rockslide-avalanche of 18 May 1980. Géotechnique 33:243–273